



ELSEVIER

Intermetallics 7 (1999) 511–528

Intermetallics

Review

Recent developments in the research of shape memory alloys

Kazuhiro Otsuka*, Xiaobing Ren

Institute of Materials Science, University of Tsukuba, Tsukuba, Ibaraki, 305-8573, Japan

Received 6 May 1998; accepted 10 June 1998

Abstract

Most of shape memory alloys are functional intermetallics. They are now practically being used for couplings, actuators, medical guide wires etc., and are hopeful candidates for smart materials, which already exist. In the present paper, recent developments within *nearly* 10 years on shape memory alloys and martensitic transformations, on which shape memory effect and superelasticity are based, were concisely reviewed. Since Ti–Ni alloys are the best practical shape memory alloys, we mostly discussed on the alloys, but we discussed more general problems as well. Furthermore, we discussed the ductility and density of point defects in intermetallics, since they are important problems in intermetallics in general. At the end we introduced some recent applications of shape memory alloys briefly. © 1999 Elsevier Science Ltd. All rights reserved.

Keywords: A. Intermetallics, miscellaneous; (B) Shape-memory effects; (G) Shape-memory alloy applications

1. Introduction

Shape memory alloys (SMA) attracted much attention in recent years, since they are smart (or intelligent) materials, as well as functional materials, which already exist. Since the unique shape memory effect (SME) and superelasticity (SE) realized in these alloys are caused by the martensitic (or displacive) transformation (MT) and its reverse transformation, we define the characteristic transformation temperatures as follows, as usual;

M_s : martensite start temperature upon cooling;

M_f : martensite finish temperature upon cooling;

A_s : reverse transformation start temperature upon heating;

A_f : reverse transformation finish temperature upon heating.

Then, SME and SE are characterized as follows, using the above terminology. SME is a phenomenon such that an apparent plastic strain given at a temperature below A_s recovers by heating to a temperature above A_f , by virtue of the (crystallographically) reversible

reverse transformation. SE, which is a pseudoelasticity occurring at a temperature above A_f , is caused by a stress-induced martensitic transformation upon loading and by the subsequent reverse transformation upon unloading. The above crystallographic reversibility is characteristic of the thermoelastic martensitic transformation, which is characterized by a small temperature hysteresis (i.e. $\Delta T = A_f - M_s$) and mobile parent-martensite interfaces. Since most of SMAs are ordered alloys or intermetallics, they are related to the present journal in that respect. In the present overview, we picked up the subjects in nearly recent 10 years, and we assumed that the readers have some introductory knowledge on MT, SME and SE. For those who are not familiar with those fundamentals, please refer to Refs. [1–4] for MT, and Refs. [5–8] for SME and SE.

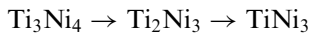
In the following, the subjects are divided into three Sections (2–4). In Section 2, recent developments in Ti–Ni based alloys are discussed, since Ti–Ni based alloys are most important SMAs and they are most actively investigated. Besides, they are distinct from other SMAs in various respects, such as in crystal structure of martensite, elastic properties, mechanical properties etc., as will be clear later. In section 3, more general properties common to all SMAs are discussed, and the applications of SMAs are discussed in the final chapter.

* Corresponding author. Tel.: +81-298-53-5294; fax: +81-298-55-7440; e-mail: otsuka@ims.tsukuba.ac.jp

2. Developments in Ti–Ni based Alloys

2.1. Phase diagram of Ti–Ni alloy system

Fig. 1 is a recent phase diagram of Ti–Ni alloy system by Massalski et al. [9] Our interests are restricted in the central region bounded by Ti_2Ni and $TiNi_3$ phases, since the single phase “TiNi” (B2 type ordered phase) transforms into a monoclinic phase martensitically. The phase diagram in the above region have been controversial for many years. The main problems are the presence or absence of a eutectoid decomposition of $TiNi \rightarrow Ti_2Ni + TiNi_3$ at $630^\circ C$ [10], and the assessment on the nature of Ti_3Ni_4 and Ti_2Ni_3 phases, which appear when a Ni-rich Ti–Ni alloy is heat-treated under suitable conditions. However, the presence of the eutectoid reaction was denied, since no experimental evidence was obtained to support it in recent studies. It was also confirmed by detailed studies by Nishida et al. [11] that Ti_3Ni_4 and Ti_2Ni_3 are metastable phases when a Ni-rich alloy is aged, and that the precipitation process occurs in the following order with ageing time until reaches a stable phase of $TiNi_3$.



Thus, the phase diagram of Ti–Ni alloy system was established as shown in Fig. 1. However, a slight modification

was added to Massalski et al.’s in Fig. 1 as described below. A dotted line at $630^\circ C$ was deleted, and a dotted line was added at $1090^\circ C$, which indicates BCC→B2 transition, following Honma [12]. Thus it is now possible to consider useful heat-treatments using this phase diagram to improve shape memory (SM) characteristics. The hardening of the parent phase by the precipitation of Ti_3Ni_4 is useful to improve SM characteristics, since they appear as thin plates in a densely dispersed manner, when they are aged at low temperature (e.g. $400^\circ C$) [13,14]. The crystal structures of Ti_3Ni_4 [15,16] and Ti_2Ni_3 [17] phases were determined also. According to the phase diagram in Fig. 1, it is not possible to expect the precipitation hardening by Ti_2Ni phase, since the phase boundary of TiNi phase on Ti-rich side is vertical and there is no change in solubility limit with lowering temperature. However, it becomes possible in Ti–Ni thin films, which are sputter-deposited in amorphous state first, and are then crystallized. This will be discussed in Section 2.7.

2.2. Crystal structures of Ti–Ni based martensites

The structure of the parent phase of Ti–Ni alloy is B2 type ordered structure. The crystal structure of binary Ti–Ni martensite has been controversial for many years since the discovery of the phase in 1961. See Ref. [18] for historical development. However, the structure was

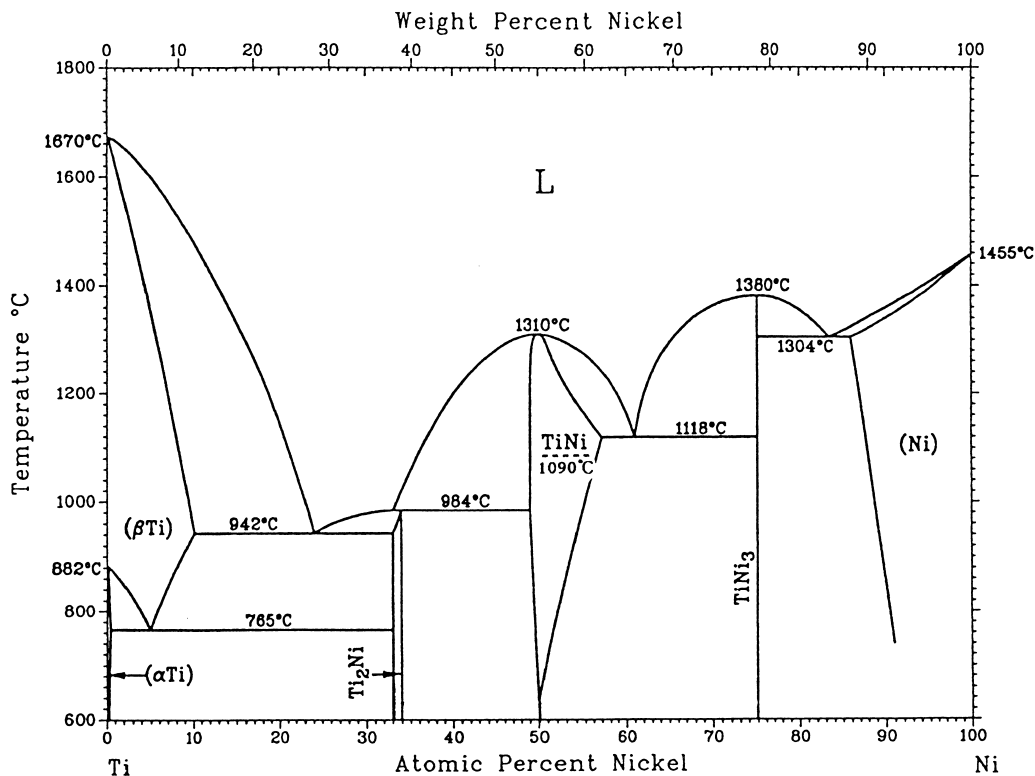


Fig. 1. Phase diagram of Ti–Ni alloy by Massalski et al. The original phase diagram is slightly modified such that a dotted line at $630^\circ C$ for eutectoid decomposition was deleted and a dotted line is added at $1090^\circ C$ for order–disorder transition for TiNi. See text for more details [9].

finally determined by using the single crystal X-ray diffraction method and by the least squares analysis [18]. The space group is $P2_1/m$ with a monoclinic unit cell. The lattice parameters and atomic parameters are given in Ref. [18], and the structure is schematically shown in Fig. 4(c). It is interesting to note that this monoclinic martensite is quite distinct from most of the martensite structures in β -phase alloys, which are long period stacking order structures of close packed planes [1,4]. Although Ti–Ni alloys are often classified as β -phase alloys, the present authors [18] consider it inappropriate to treat that way, since the electron/atom ratio (e/a) is far from 1.5 in Ti–Ni alloys, which is required for the β -phase alloy.

When 2–3 at% Ni is replaced by Fe or Al in the Ti–Ni binary alloy, the R-phase transformation with a very small temperature hysteresis ($\sim 2\text{K}$) occurs prior to the above martensitic transformation [19,20]. The same R-phase transformation is realized in Ti–Ni binary alloys by suitable thermomechanical treatments [21]. The transformation is called the R-phase transformation, since the lattice changes from cubic to rhombohedral upon the transformation, i.e. the rhombohedral lattice is obtained by elongating the cubic lattice along $\langle 111 \rangle_{B2}$ (see Fig. 2). This transformation is very useful for actuator applications, since it is associated with a very small temperature hysteresis, as described above. This structure has also been controversial for many years, but it has recently been determined by the combination of various techniques such as electron diffraction, X-ray powder method etc. [23]. The space group is $P3$, which has no center of symmetry, and the lattice parameters and atomic parameters are given in Ref. [23]. The structure is very similar to that of ζ'_2 martensite in a Au–Cd alloy [24]. See Refs. [23,25] for historical developments.

2.3. Premartensitic phenomena

Nucleation mechanism of martensite is a long-standing problem. Premartensitic phenomena to be described below attract attention in this respect. Some thermoelastic alloys exhibit significant change in physical properties in certain elastic constants and phonon dispersion curves in the parent phase with decreasing temperature, e.g. in most of β -phase alloys the elastic constant $c' = 1/2 (c_{11} - C_{12})$ decreases with decreasing temperature toward M_s [26]. When the change in the parent phase is important for the subsequent martensitic transformation, it is called a premartensitic phenomenon. These phenomena are interesting in Ti–Ni based alloys as well, but the measurements were rather few in the past [27–29], since single crystals are not easily available in Ti–Ni alloys. In the following, we introduce recent measurements of various elastic constants as a function of temperature for Ti–30Ni–20Cu

and Ti–50Ni single crystals, in which the former transforms from B2 to B19 (orthorhombic), while the latter from B2 to B19' (monoclinic) (Fig. 3) [30]. We immediately notice from the figure that both c' and c_{44} decrease with decreasing temperature toward M_s . Of course, this temperature dependence is opposite to that of ordinary non-transforming materials. Here c' represents a resistance for $\{110\}\langle 111 \rangle$ shear, and c_{44} a resistance for $\{001\}\langle 100 \rangle$ shear, which is also equivalent to a resistance

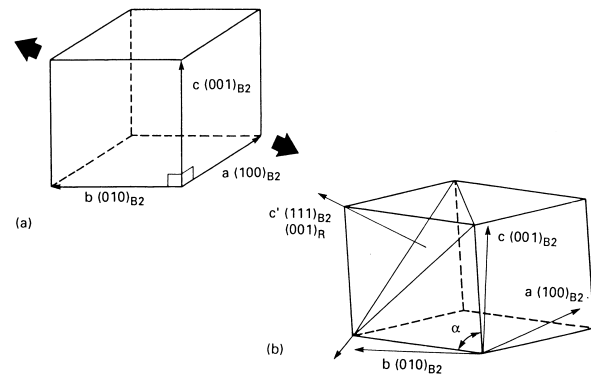


Fig. 2. Lattice change associated with the R-phase transformation. (a) The B2 type parent phase and (b) the R-phase [22].

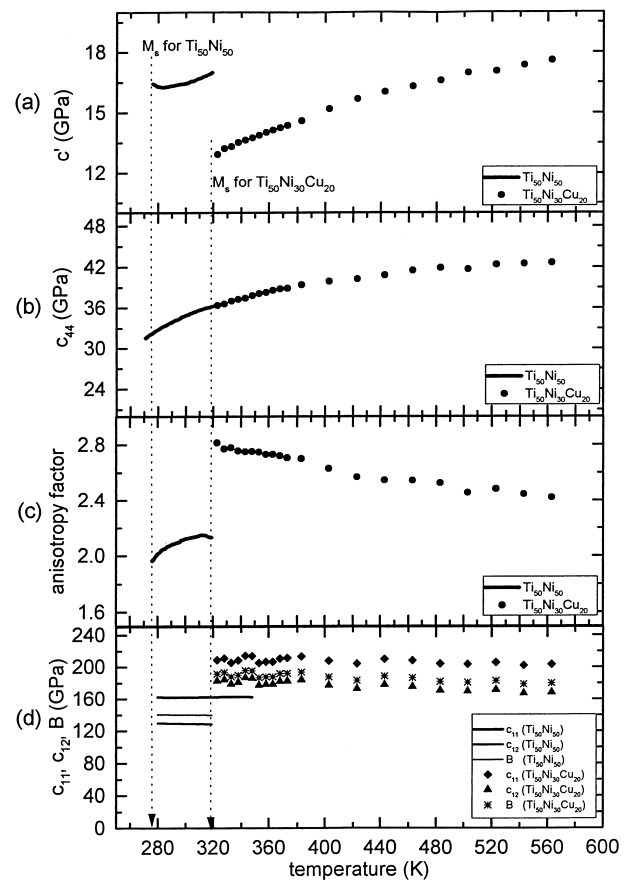


Fig. 3. Temperature dependence of (a) c' , (b) c_{44} , (c) anisotropy factor and (d) c_{11} , c_{12} , B for Ti–30Ni–20Cu and Ti–50Ni alloys [30].

for $\{001\}\langle 1\bar{1}0\rangle$ shear. Fig. 4 shows a structural relationship between B2 parent and B19 martensite, and B19' martensite. By comparing Fig. 4(a) and (b), it is clear that $\{110\}\langle 1\bar{1}0\rangle$ shear is necessary to create B19 structure from B2 parent structure. Thus, the softening in c' assists the structure change from B2 to B19. However, for the structural change from B2 to monoclinic B19', $\{110\}\langle 1\bar{1}0\rangle$ shear above is not enough. Instead $\{001\}\langle 1\bar{1}0\rangle$ shear is also necessary, as seen from Fig. 4(c). Thus, the simultaneous softening in c' and c_{44} assists the transformation from B2 to B19' monoclinic martensite. Thus the present authors recently proposed that the appearance of B19' monoclinic martensite is due to the softening in c_{44} , as described above [31]. However, you will notice soon that although c_{44} softens with decreasing temperature both in Ti–50Ni and Ti–30Ni–20Cu, only the former transforms into monoclinic martensite and the latter into orthorhombic one. This point is

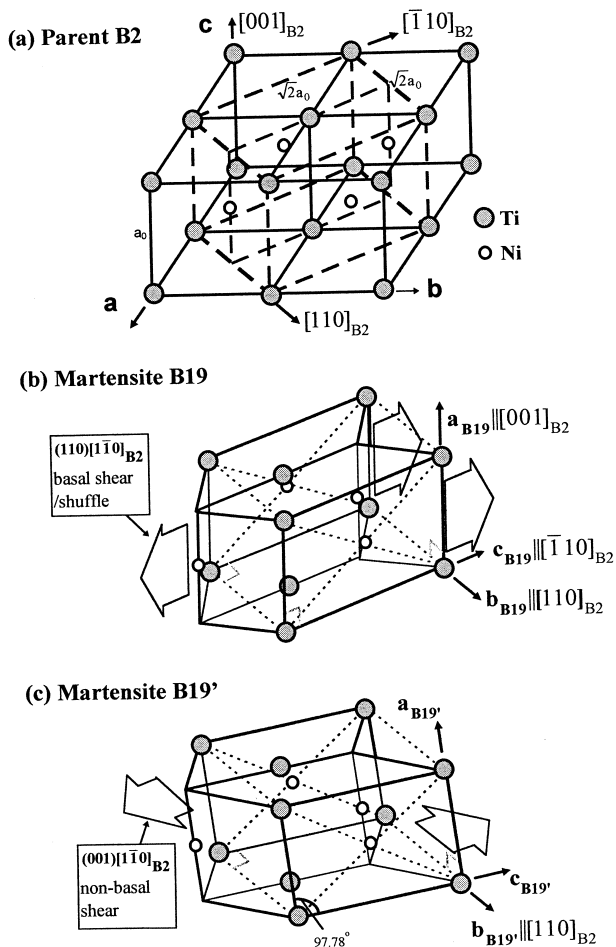


Fig. 4. Structural relationship among cubic parent phase (B2) and two kinds of martensites B19 and B19'. (a) The parent B2 cells with a FCT cell outlined, where close-packed planes or basal planes are indicated with thin dashed lines; (b) orthorhombic martensite B19, formed by shear/shuffle of the basal plane $(110)_{B2}$ along $[1\bar{1}0]_{B2}$ direction; (c) monoclinic B19' martensite of Ti–Ni, formed by a non-basal shear $(001)[1\bar{1}0]_{B2}$ to the B19 structure to produce a monoclinic β angle [31].

rationalized as follows. According to Fig. 4(c), the anisotropy factor $A = c_{44}/c'$ decreases with decreasing temperature in Ti–50Ni, while it increases with decreasing temperature in Ti–30Ni–20Cu. i.e. c' and c_{44} become comparable in the former, while c' becomes dominant in the latter with decreasing temperature. The authors think that this difference makes the difference in martensite structures between monoclinic and orthorhombic [31]. In short, the appearance of the unique monoclinic martensite in Ti–Ni alloys are due to the very low anisotropy factor and its temperature dependence, where A decreases with decreasing temperature toward M_s . Some interesting results are being obtained on the relation between phonon softening and the structural change. See also Ref. [26,32] for elastic constants behavior in β -phase alloys.

2.4. Ti–Ni–X (X = Cu, Nb etc.) ternary alloys

To change transformation temperature, physical properties or mechanical properties, various ternary alloys are being developed. Among these, Ti–(50–x)Ni–xCu and Ti–Ni–Nb alloys are most important from the reasons described below.

The addition of Cu exhibits various interesting effects as shown in Figs. 5 and 6 [33]. Firstly, there is no appreciable change in the transformation temperature with change in Cu content. Secondly, the transformation type changes with increasing Cu content; $\text{Cu} \leq 7.5$:

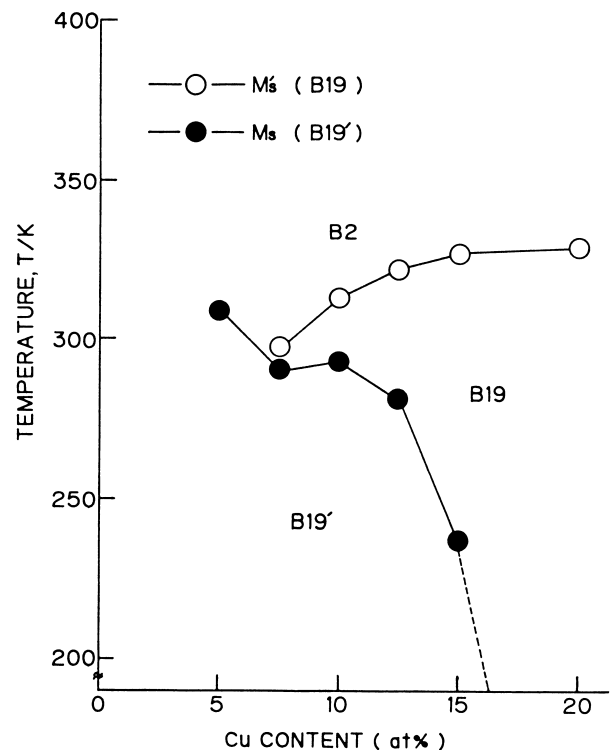


Fig. 5. Effect of Cu content on the martensitic transformations of Ti–(50–x)Ni–xCu alloys [33].

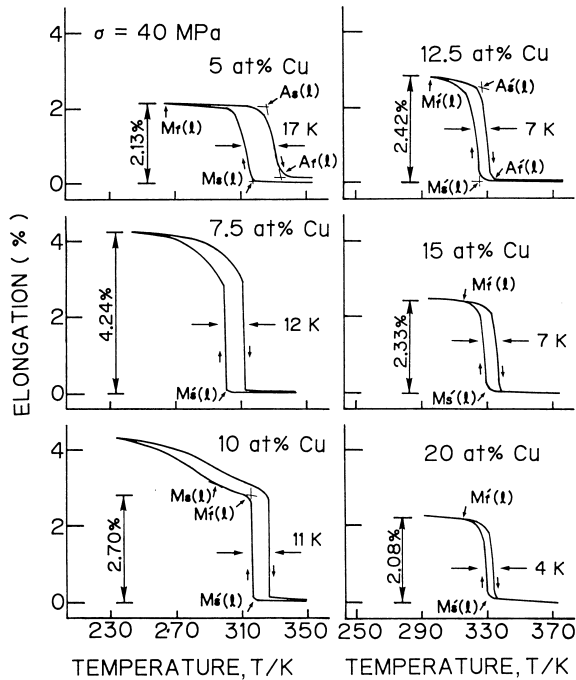


Fig. 6. Elongation(ϵ)-temperature(T) curves under the nearly same load (about 40 MPa) for Ti-(50- x)Ni- x Cu alloys [33].

B2→B19', 7.5 < Cu ≤ 15: B2→B19→B19', Cu ≥ 15: B2→B19 only. The B2→B19 transformation is associated with a smaller temperature hysteresis than that for B2→B19', and the transformation hysteresis becomes smaller with increasing Cu content. In this respect, Ti-Ni-Cu alloys are useful for actuator applications. With respect to the temperature hysteresis, the above mentioned R-phase transformation is associated with the smallest temperature hysteresis, but the associated shape memory strain is also small (~1%). However, the Ti-Ni-Cu alloys are associated with larger shape memory strains as shown in Fig. 6, and they can be used at a slightly higher temperature range compared to those of the R-phase transformation.

When SMAs are used for actuator applications, smaller temperature hysteresis is desirable, as stated above. However, when they are used for coupling applications, larger temperature hysteresis is better, because the deformed couplings in the martensitic state can be stored easily at room temperature. In this respect, Ti-Ni-Nb alloys are most useful, especially because the A_s temperature is raised significantly when the alloy is deformed in the martensitic state. However, this mechanism will be discussed in more general terms in Section 3.3. See Refs. [34–36] for more details on Ti-Ni-Nb alloys.

2.5. Twinning in Ti-Ni martensites

Twinning in martensites are very important with respect to martensite crystallography and deformation

modes. The crystallography of B2→B19' transformation was studied in detail based on "the phenomenological theory of martensitic transformations", and it is not repeated here [37]. The self-accommodation mechanism by the combination of multiple martensite variants, is also studied for both B2→B19' [38] and B2-R [39] transformation. Although the self-accommodation of the R-phase is well understood, that of B19' is a little controversial.

Table 1 lists various twinning modes in B19' martensite. It is interesting to note that there are many twinning modes. This is because the symmetry of the martensite is lower than ordinary martensites. Among these, {011} Type II twinning is most important, since it is the lattice invariant shear in the B2→B19' martensite crystallography, which is necessary to make the parent-martensite interface macroscopically invariant [37,41]. Type II twinning is characterized by an irrational K_1 (twin) plane, and the two twin crystals are related by a rotation of π around η_1 axis (i.e. twinning shear direction). There is a suggestion that the irrational K_1 plane consists of rational ledges and rational steps [41]. However, in the high resolution electron micrograph of Fig. 7, which was taken in the unique axis of η_1 , we can not see a ledge nor a step [42]. We think that the Type II twin interface is irrational even on a microscopic scale, and the twinning strain is accommodated elastically at the interface [42,43].

2.6. Ductile nature of intermetallic Ti-Ni alloys

The ductility of Ti-Ni alloys is quite remarkable among many intermetallics, which are usually brittle. As typically shown in Fig. 8 elongation more than 50% is easily obtained. Thus, the discussion will be useful for improving ductility in other intermetallics. The temperature dependence of elongation is important, as shown in Fig. 9. It indicates that elongation becomes maximum around the M_s temperature. This is a clear manifestation that the high ductility is closely related with the presence of the martensitic transformation. We now raise various factors, which assist the high ductility in the alloy system.

1. There are 24 habit plane variants upon stress-induced martensitic transformation. This means that there are 24 deformation modes upon stress-induced transformation.
2. There are many twinning modes in the martensite, as listed in Table 1.
3. Anisotropy factor A is as low as ~ 2 in Ti-Ni alloys. Thus the grain boundary fracture due to elastic anisotropy may be avoided.
4. Grain size is usually very small. Typically $\sim 30 \mu\text{m}$. This is in sharp contrast to those of β -phase alloys, which are typically $\sim 1 \text{ mm}$.

Table 1
Twinning modes of Ti–Ni martensite [40]

Twinning mode	K_1	η_1	K_2	η_2	s	Sol. ^a
$\{\bar{1}\bar{1}\}$	$(\bar{1}\bar{1})$	$[0.54043 \ 0.45957 \ 1]$	$(0.24695 \ 0.50611 \ 1)$	$[\bar{2}\bar{1}]$	0.30961	yes
Type I	$(\bar{1}\bar{1})$	$[0.54043 \ 0.45957 \ 1]$	$(0.24695 \ 0.50611 \ 1)$	$[\bar{2}\bar{1}]$	0.30961	yes
$\{111\}$	(111)	$[1.51172 \ 0.51172 \ 1]$	$(0.66875 \ 0.33750 \ 1)$	$[211]$	0.14222	no
Type I	(111)	$[1.51172 \ 0.51172 \ 1]$	$(0.66875 \ 0.33750 \ 1)$	$[211]$	0.14222	no
$\{011\}$	(011)	$[1.57271 \ 1 \ \bar{1}]$	$(0.72053 \ 1 \ \bar{1})$	$[011]$	0.28040	yes
Type I	$(01\bar{1})$	$[1.57271 \ 1 \ 1]$	$(0.72053 \ 1 \ 1)$	$[0\bar{1}\bar{1}]$	0.28040	yes
$\langle 011 \rangle$	$(0.72053 \ 1 \ \bar{1})$	$[011]$	(011)	$[1.57271 \ 1 \ \bar{1}]$	0.28040	yes
Type II	$(0.72053 \ 1 \ 1)$	$[0\bar{1}\bar{1}]$	$(0\bar{1}\bar{1})$	$[1.57271 \ 1 \ 1]$	0.28040	yes
Compound	(001)	$[100]$	(100)	$[001]$	0.23848	no
	(100)	$[001]$	(001)	$[100]$	0.23848	no

^a Existence of a solution for the phenomenological crystallographic theory.

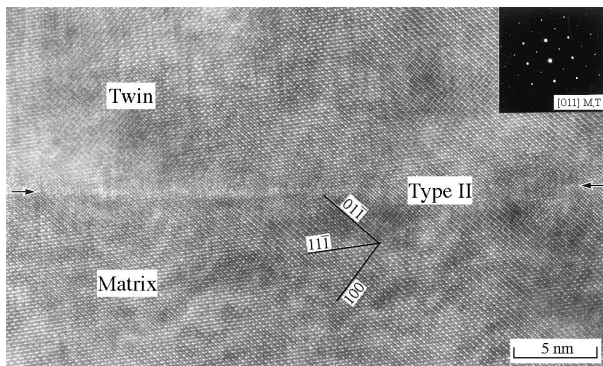


Fig. 7. High resolution electron micrograph of $\langle 011 \rangle$ Type II twin boundary taken from the $\eta_1 // [011]$ unique axis. See text for details [42].

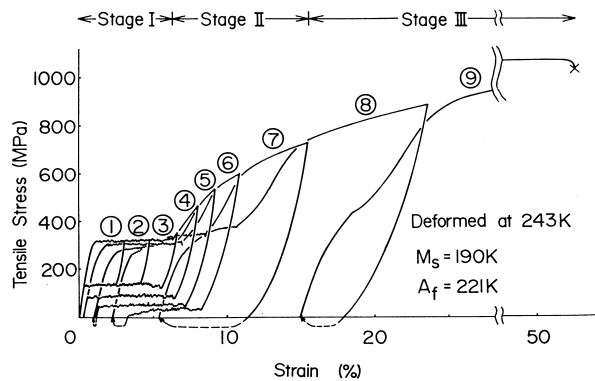


Fig. 8. Tensile stress–strain curves of Ti–50.6Ni alloy deformed at 243 K ($> A_f$). Dotted lines represent the recovered strain upon heating to 373 K. The symbol (x) represents the fracture point [44].

- The critical tensile stress for slip is very low at M_s (less than 50 MPa), while that in the parent phase for the same single crystal is about 400 MPa [45].

In fact, the combination of these factors make the Ti–Ni very ductile, e.g. If only the item 1 is important, then we can expect that all β -phase alloys exhibiting the

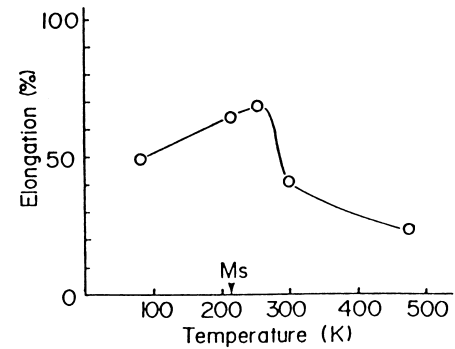


Fig. 9. Temperature dependence of the elongation of Ti–51Ni alloy [45].

martensitic transformation are ductile. However, most of the β -phase alloys are quite brittle, because the anisotropy factor is usually as high as 10–15, the grain size are large and the critical stress for slip are usually high. Thus, we can now understand that the ductility of Ti–Ni alloy system is based on the availability of these various factors.

According to Fig. 9, the ductility decreases at high temperatures in the parent phase significantly, but it is still higher ($\sim 20\%$) compared to those of most intermetallics. Since stress-induced transformations and twinning in martensites do not contribute to ductility at such high temperatures the high ductility may be explained as follows. Firstly, items 3 and 4 are still valid at high temperatures. Secondly, we focus attention on the low value of elastic constant c_{44} in Ti–Ni based alloys, which was shown in Fig. 3(b). In fact, c_{44} in Ti–Ni based alloys are smaller than 1/3 of that of other B2 type intermetallics with similar melting point such as Ni–Al. The abnormally low c_{44} leads to a low Peierls stress for $\{110\}\langle 001 \rangle$ slip system, which is the operating system in Ti–Ni alloy [46]. Thus, the combination of items 3 and 4, and the low value of c_{44} may be the origin for the high ductility at high temperatures. Besides, there is a report that $\{112\}$ and $\{114\}$ twinning modes

are present even in the parent phase [47], which increase the available deformation modes. Apparently these also assist to increase in ductility in the parent phase. However, there may be a possibility that these twins were introduced by stress-induced transformation, since mechanical twinning in ordered alloys do usually not operate easily [48,49]. These points should be examined more carefully.

2.7. Ti–Ni thin films

By the expected applications for microactuators and micromachines, various techniques were tried for the fabrication of Ti–Ni thin films, including rapid quenching technique [50], and it is now possible to make thin films rather easily by magnetron sputtering technique [51–65]. Thus active investigations are being done on the microstructures and mechanical properties. In the magnetron sputtering technique, Ti–Ni alloys are used as a target, and the composition is adjusted by placing Ti plates on the target, and the substrate is either a glass or a quartz plate. The characteristic of the Ti–48.7at%Ni film thus made is shown in Fig. 10, as an example. The as-sputtered film on a glass substrate at 523 K is in amorphous state. When the film is heated to a temperature above the crystallization temperature (~ 723 K), it crystallizes, and then it exhibits the martensitic transformation. In the present case, the crystallization treatment was done at 973 K for 1 h. The data in the figure are temperature-elongation curves under constant stress, e.g. Under 30 MPa, 1% elongation is obtained by the martensitic transformation between M_s and M_f . Upon heating this strain is recovered. This is the shape memory effect. We notice that the strain increases with increasing stress. This is because particular variants favorable to the stress are stress-induced under higher stress. Under high stresses, the strain upon cooling and that upon heating becomes unequal. This is due to the introduction of slip in the reverse transformations [66],

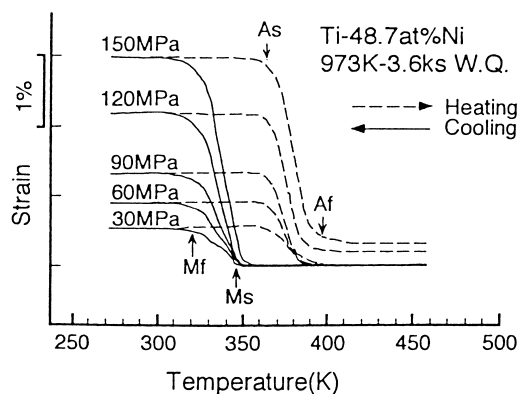


Fig. 10. Strain-temperature curve of Ti–48.7Ni thin film under various constant loads. Crystallization and solution-treatment were carried out at 973 K for 3.6 Ks [53].

i.e. SME becomes incomplete under higher stresses. The shape memory characteristics and the transformation behavior in thin films are similar to those in bulk materials. However, the films crystallized from amorphous state have very small grain size ($\sim \mu\text{m}$ to sub- μm), and thus have good mechanical properties. Furthermore, since the as-sputtered films are in amorphous state, they can absorb solute atoms more than the solubility limit. Thus, it is possible to control microstructures by precipitation on Ti-rich side also. We will introduce an interesting case in that respect as follows.

According to the phase diagram of Fig. 1, the solubility limit of Ni increases with increasing temperature on Ni-rich side. Thus, it was possible to strengthen the parent phase of Ti–Ni by utilizing the metastable Ti_3Ni_4 precipitate, and this technique was practically utilized to improve the shape memory characteristic of Ni-rich Ti–Ni alloys in bulk [13,14]. On the other hand, the precipitation hardening could not be used on Ti-rich side, since the solubility limit does not change with temperature. However, since it is possible to absorb Ti freely (i.e. more than the concentration of the solubility limit in crystalline state) in amorphous state, it is possible to use the precipitation hardening even on Ti-rich side, if the Ti-rich alloy is solidified in amorphous state, followed by crystallization and ageing. Furthermore, it was found recently that Ti-rich GP zones precipitate along $\{100\}_{\text{B}_2}$ planes [56,61,62] (Fig. 11), if the films are crystallized at low temperatures, although the equilibrium precipitate is Ti_2Ni phase, and the shape memory characteristics improve greatly by that precipitation hardening [61]. As an example, the case for Ti–48.2at%Ni alloy is shown in Fig. 12, which is to be compared with Fig. 10. It is easy to see that the shape memory strain and the stress, for which SME is observed, is improved greatly. Although there are more interesting points for



Fig. 11. High resolution TEM image of a sputter-deposited Ti–48.5at%Ni thin film annealed at 773 K for 600 s, observed along $[001]$ direction of B_2 parent phase. GP zones coherent to the B_2 matrix are present along (100) and (010) planes [67].

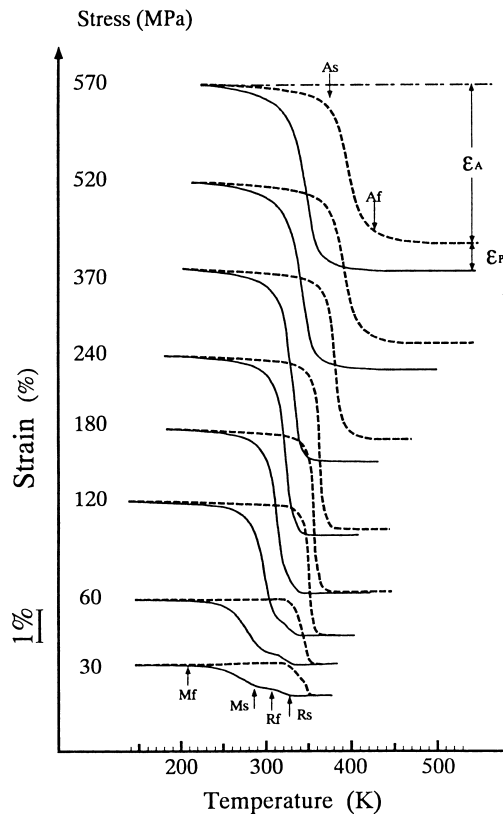


Fig. 12. Strain-temperature curves of Ti-48.2Ni thin film under various constant stresses containing GP zone precipitates. The specimen was heat-treated at 745 K for 1 h, which is slightly above the crystallization temperature 737 K [61].

this precipitation on Ti-rich side, refer to the original papers for those.

Thus, it has become possible to make Ti-Ni thin films with good mechanical properties, but one problem for practical use is the control of the composition of thin films [65]. Since it seems that the composition is different even on the same substrate and the transformation temperature is very sensitive to composition, composition control will be an important problem in the future. Furthermore, for the application to micromachines, the substrate must be Si chips. Thus, how to avoid the constraint due to the large difference in the thermal expansion coefficient of the thin film and substrate will be the second problem [65]. As the third, we expect further development of applications of thin films, since many applications are not disclosed as yet [68].

3. Developments in shape memory alloys in general

3.1. Defect densities in intermetallics—are there any constitutional vacancies in intermetallics?

As mentioned earlier, most of SMAs are in fact intermetallic compounds (shape memory intermetallics)

because they are ordered alloys and many of them remain ordered near to the melting temperature (e.g. Ti-Ni, Au-Cd, etc.). Therefore, point defects we discuss here include both vacancy and anti-site defect (ASD).

In comparison to the relatively recent knowledge about the role of point defects on mechanical properties of structural intermetallics for high temperature applications [69], the important role of point defects in shape memory intermetallics has been widely known for many decades, because they strongly affect nearly all aspects of martensitic transformation. This is evidenced by the strong dependence of M_s temperature, transformation hysteresis, and even the structure of martensite, on the concentration of point defects, which can be varied either by composition change or by heat-treatment (e.g. quenching). For example, in many alloys (e.g. Cu-Zn, Ti-Ni, Cu-Al, Fe-Pd, ...) only 1 at% change in composition varies the M_s temperature by as much as tens of or even over a hundred degrees. Sometimes a very small change in composition can even change the resultant martensite structure (e.g., Au-47.5Cd and Au-49.5Cd have different martensite structure). Quenching also gives rise to strong change in transformation temperature and even change in martensite structure, as well as an increase in transformation hysteresis. Point defects also play a central role in determining the puzzling martensite aging effect, which will be discussed in the next section.

Lattice dynamics plays a key role in martensitic transformations, as manifested by frequently observed lattice softening prior to martensitic transformation [70,71] Therefore, we expect that the effect of point defects on MT must stem from their influence on lattice dynamics through changing elastic constants and phonon energies, as well as anharmonic energies. A typical example of this has been given in Section 2.3, which showed how an addition of Cu to Ti-Ni changes the elastic constants and ultimately the structure of martensite.

Despite the importance of point defects, quantitative information about their concentrations and composition dependence in SMAs (intermetallics) is rare. This may be due to the experimental difficulty in measuring defect concentrations. Only Au-Cd furnace-cooled β_2 alloy has been measured systematically in its whole homogeneity range (Cd = 46~52 at%) [72], as shown in Fig. 13. The vacancy concentration is determined by a combination of density measurement and x-ray lattice parameter determination, and the concentrations of other defects (Au-ASD and Cd-ASD) are determined by best-fitting the experimental vacancy-composition relation with a theoretical model. A notable fact from this result is that vacancy concentration in slow-cooled Au-Cd is rather high ($> 10^{-3}$), and is extremely high on Cd-rich side ($\sim 10^{-2}$), compared with that in pure metals or disordered alloys even in their quenched state. This feature is common to many intermetallics with the open B2 structure.

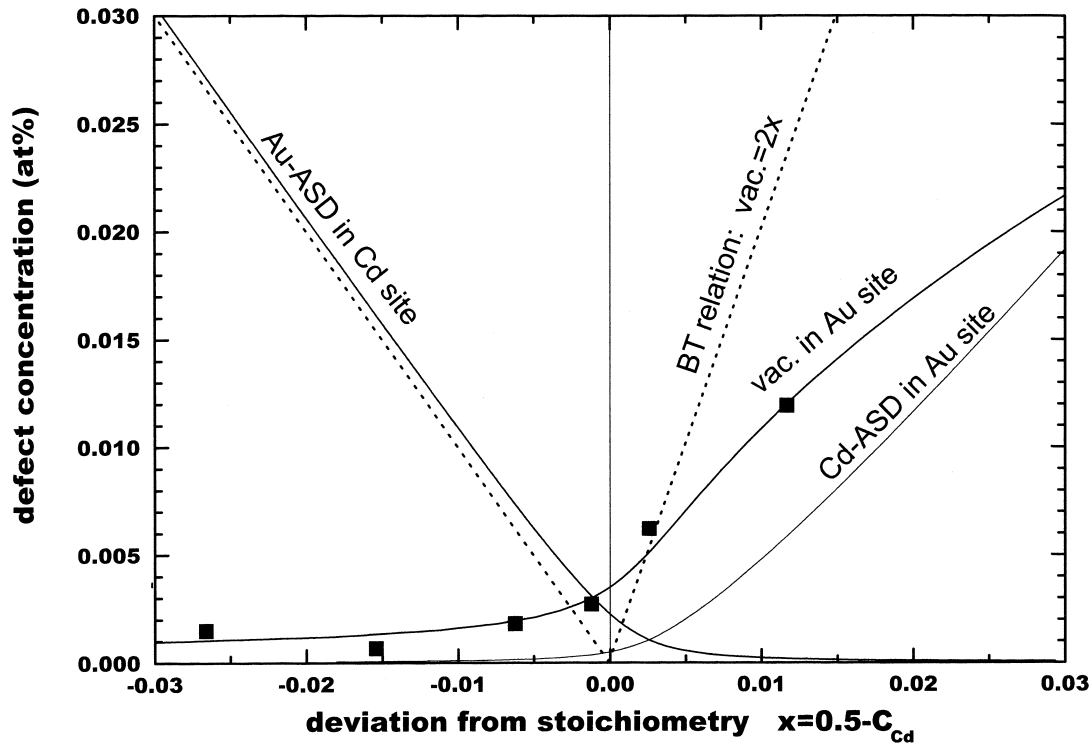


Fig. 13. Composition dependence of point defect (vacancy/ASD) concentrations for Au–Cd alloys [77]. Experimentally measured vacancy concentrations are shown with square symbol [72].

Intermetallics are usually divided into three distinct types according to their defect types [73]: triple defect (TRD) type, ASD type and hybrid type. For TRD type intermetallics (e.g. Ni–Al, Co–Al, Fe–Al) vacancy is thought to be a necessary constituent to stabilize the B2 structure, thus a very high concentration of vacancy is considered to be stable down to absolute zero. The minimum vacancy concentration z for TRD intermetallics is $z = 2x$ on one side from stoichiometry (where x is the composition deviation from stoichiometry) as shown by the Bradley–Taylor (BT) [87] line in Fig. 1. Such stable vacancy is usually called ‘constitutional vacancy’. On the other hand, in ASD type and hybrid intermetallics vacancy is unstable at low temperatures, thus its concentration is below BT line. Au–Cd apparently belongs to the hybrid type and it contains a large amount of frozen-in vacancy.

For over 60 years it has been widely believed that TRD intermetallics such as Ni–Al, Co–Al and Fe–Al contain constitutional vacancies. However, recent careful measurements on these intermetallics found that even these ‘typical’ TRD intermetallics have vacancy concentration appreciably below the BT-line [74–76], which is the lower limit for constitutional vacancy to exist. This behavior is qualitatively similar to the case of Au–Cd. This clearly suggests that vacancy is unstable at low temperature, thus gives a strong challenge to the notion of constitutional vacancy. Based on these experimental findings, we showed that no constitutional

vacancy exists in any intermetallics, and the difference in vacancy-frozen temperature (which depends on ordering energy) gives rise to three apparently different types of intermetallics [77].

3.2. Martensite aging effect—stabilization and rubber-like behavior

Martensite aging effect is a puzzling phenomenon unclear for over 60 years, and has been found in Au–Cd, Au–Cu–Zn, Cu–Zn–Al, Cu–Al–Ni, and In–Ti. It involves two time-dependent phenomena during martensite aging. One is called martensite stabilization, the other is called rubber-like behavior (RLB). Martensite stabilization refers to the phenomenon that martensite appears to be more stable with respect to the parent phase during aging so that the reverse transformation temperature is increased. The rubber-like behavior refers to the phenomenon that martensite exhibits a recoverable or pseudo-elastic deformation behavior after aging together with an increase in critical stress, as exemplified in Fig. 14(A). The most puzzling problem with the RLB is why there should exist a restoring force, because martensite deformation involves only twinning and there is no phase transformation involved, unlike that of superelasticity of the parent phase due to stress-induced martensitic transformation. The microstructure change underlying the RLB is a reversible one, that is, the original martensite domain pattern is recovered after

unloading Fig. 14(B) (The term ‘variant’ is more common than ‘domain’ in the field of martensite. However, the former is used in the present paper for easy understanding of non-specialists.). This is even true for single-domain martensite which does not contain twin boundaries, [78], suggesting that the RLB is not a boundary effect. The central question concerning the martensite aging effect is: what is occurring during martensite aging, which gives rise to stabilization and the RLB?

In past decades, there have been numerous studies trying to clarify the origin of the martensite aging effect (see Ref. [79] for a recent review). However, a general mechanism applicable to all martensites was not found. For example, the existence of aging effect in single domain martensite [80,81] (i.e. without twin boundary) proved that the boundary-pinning mechanism is inappropriate. Many previous studies using Cu-based alloys concluded that some structure change (more or less depending on model) during aging in martensite is necessary to cause the aging effect. However, martensites of these alloys are unstable (i.e. not equilibrium phases), and thus they have an inborn tendency to decompose simultaneously during aging. Therefore, the observed structure change may be just due to the inad-

vertent decomposition, while aging itself may be independent of the decomposition. Recent extensive experiments on stable martensites Au–Cd [78,82] and Au–Cu–Zn [83] (without decomposition problem) proved that aging develops even without any detectable change in average martensite structure (Fig. 15). This seemingly perplexing result is in fact very natural, since the average structure of an equilibrium or stable phase is not expected to depend on time (aging). Then the remaining puzzle is how a significant change in mechanical properties and transformation behavior can be realized without leading to average structure change. Ahlers et al. tried to explain the aging effect by a short range ordering (SRO) model [84] which was later extended further by Marukawa and Tsuchiya [85], but the occurrence of such SRO would necessarily lead to some atomic exchange between different sublattices of martensite and thus lead to appreciable change in long range order or average structure of martensite. Obviously, this contradicts experimental results.

The answer to this puzzle was given very recently by Ren and Otsuka [86]. They showed that the aging phenomena stem from a general tendency that the symmetry of short-range order configuration of point defects tries to conform or follow the symmetry of the crystal. This is named symmetry-conforming short-range order principle (or SC–SRO principle) of point defects, and is applicable to any crystal containing point defects.

The SC–SRO principle gives a general and simple explanation to the aging phenomena. Fig. 16(a) shows a two-dimensional A–B binary imperfectly-ordered parent phase with four-fold symmetry. Because of the four-fold symmetry of the structure, the probability of finding a B atom about the A atom (or B atom) must possess the

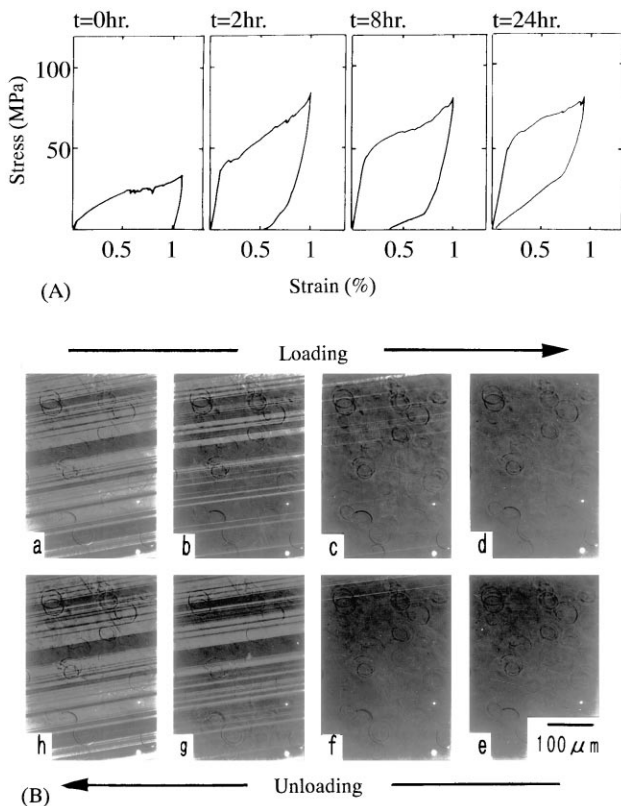


Fig. 14. Demonstration of the rubber-like behavior. (A) Represents the change of stress–strain curves of a furnace-cooled Au–47.5Cd alloy (a single crystal in the parent phase) after aging in martensite for various times t . (B) Represents the change in twin patterns of the martensite during loading and unloading of the martensite after aging for more than 24 h.

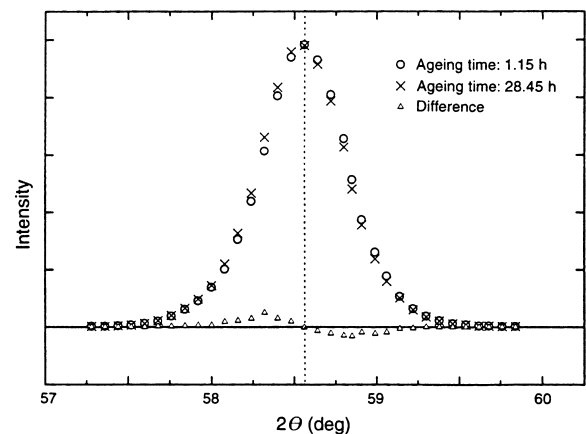


Fig. 15. X-ray profiles of (242) Bragg reflection of Au–47.5%Cd martensite after aging for short (1.15 h) and long (28.45 h) time, respectively. No perceptible change in peak position and integrated intensity was found during aging. However, a delicate change in the symmetry of the profile was found to develop during aging, as manifested by the difference of the two profiles [82].

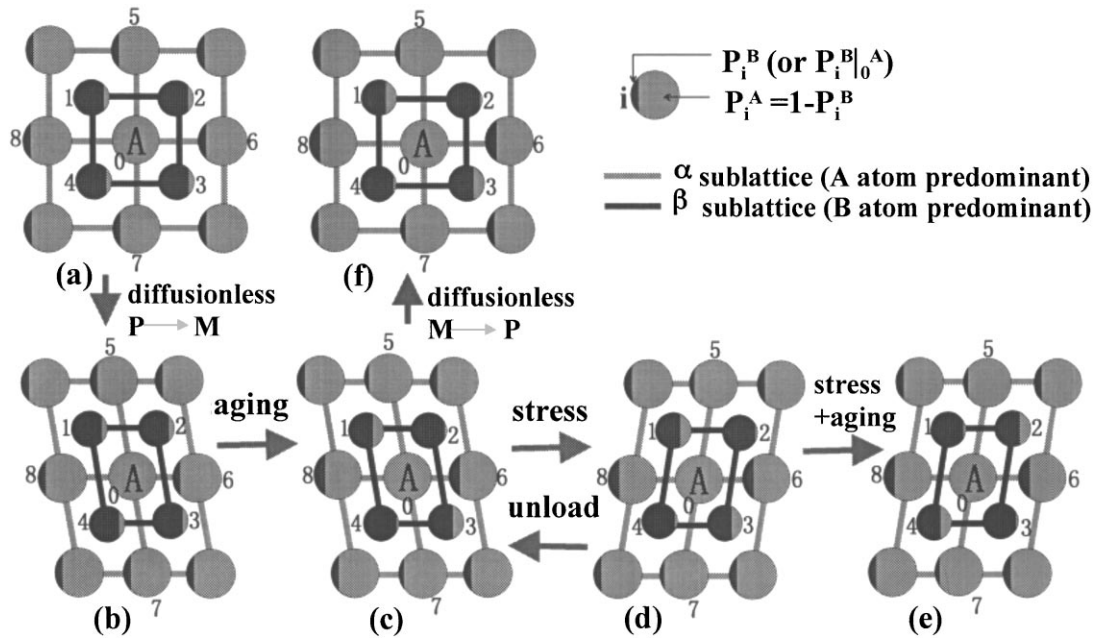


Fig. 16. Mechanism of the rubber-like behavior and martensite stabilization phenomenon. The illustrations show the statistical atomic configuration (conditional probabilities around an A atom) of an imperfectly-ordered AB compound in, (a) equilibrium parent phase; (b) martensite immediately after transformed from (a); (c) equilibrium martensite; (d) stress-induced martensite domain (twin) immediately formed from (c); (e) equilibrium state of the stress-induced domain; and (f) parent immediately transformed from (c), respectively. P: the parent phase, and M: martensite. P_i^B (or P_i^A) is the conditional probability of B atom (or A atom) occupying i -site ($i = 1, 2, 3, \dots, 8$) if an A atom is at O-site. The relative values of P_i^B and P_i^A are indicated by the black and grey areas, respectively [86].

same four-fold symmetry according to SC-SRO principle, i.e., $P_1^B = P_2^B = P_3^B = P_4^B$, and $P_5^B = P_6^B = P_7^B = P_8^B$, etc., where P_i^B ($i = 1, 2, 3, \dots$) are conditional probabilities, as defined in Fig. 16.

When the parent phase shown in Fig. 16(a) transforms diffusionlessly into martensite, all the probabilities must remain unchanged despite the symmetry change, as shown in Fig. 16(b). That is, $P_1^B = P_2^B = P_3^B = P_4^B$, and $P_5^B = P_6^B = P_7^B = P_8^B$, etc.. However, this high-symmetry configuration is no longer a stable configuration for the lower symmetry martensite structure according to the SC-SRO principle. Then during aging, such a configuration gradually changes into a stable one that conforms to martensite symmetry, as shown in Fig. 16(c). Because the equilibrium martensite structure should be maintained (for stable martensite), this process proceeds by atomic rearrangement or relaxation within the same sublattice. This is the only way that a martensite can lower its free energy without altering the average structure (equilibrium phase).

When the stabilized (or aged) martensite [Fig. 16(c)] is deformed, it changes into another domain (or twin) as a result of the accommodation of the strain. Because this twinning process is also diffusionless, the atomic occupation probabilities shown in Fig. 16(c) is inherited to the new domain, as shown in Fig. 16(d). Such a configuration, however, is not the stable one for the new domain, which is shown in Fig. 16(e). Therefore, a driving force that tries to restore the original domain

[Fig. 16(c)] engenders. When the external stress is released immediately after the loading, this restoring force reverts the new domain [Fig. 16(d)] to the original one [Fig. 16(c)] by detwinning. This is the origin of the rubber-like behavior. If the stress is held for some time, atomic configuration in Fig. 16(d) have enough time to change into a stable configuration [Fig. 16(e)], then no RLB will occur.

When the stabilized martensite [Fig. 16(c)] is heated up and transforms back (diffusionlessly) into the parent, the stable SRO configuration for the martensite is inherited into the parent [Fig. 16(f)]. From the above-mentioned symmetry-conforming principle of SRO, it is obvious that Fig. 16(f) is not a stable configuration for the parent. From a thermodynamic point of view, this corresponds to an increased reverse transformation temperature. This is the origin of martensite stabilization.

The SC-SRO model can be easily extended into disordered alloys by considering the existence of only one sublattice. In this case, the present model reduces to Christian's model [88], which was later elaborated by Otsuka and Wayman [6]. This model explained the rubber-like elasticity in disordered alloys such as In-Tl.

The largest advantage of the SC-SRO model compared with previous models is its generality. It not only explains why aging does not cause a change of average structure of martensite, but also unified the origin of aging effect for both ordered and disordered martensites.

The generality of the model lies in that it makes use of only two general features of martensitic transformation and aging: diffusionless symmetry-change upon martensitic transformation and (short-range) diffusion of point defects during aging. In line with this reasoning, it can be deduced that the existence of point defects and possibility of diffusion in martensite are two necessary conditions for aging phenomena. The existence of point defect is generally satisfied by alloys, but the possibility of diffusion in martensite depends on the reduced martensitic transformation temperature M_s/T_m , where M_s and T_m are martensite start temperature and melting point of the alloy. The higher this reduced temperature is, the faster diffusion in martensite becomes. If this value is too low, aging phenomena are too slow to be observed; if this value is too high, aging is so fast that aging actually completes immediately after the martensitic transformation, thus the time-dependence of aging may not be observed. As shown in Table 2 [79], Ti–Ni alloy belongs to the former case, and In–Tl belongs to the latter. Other shape memory alloys are in-between. Thus we give an answer to an important problem as to why some alloys show strong aging effect, while others show little. The absence of martensite aging effect in Ti–Ni shape memory alloys [91] is very interesting, because this property is desirable for most applications of SMAs. The reason, as stated above, is very simple. This reminds us that the most effective way to develop SMA without aging effect is to choose alloys with low M_s/T_m value. This can be realized by (i) using SMA with a low M_s , or (ii) using SMA with high T_m . Since the first method are usually restricted by application purpose, using alloys with high melting temperature becomes the most effective method. Therefore, the development of SMA without aging effect should focus on alloys with high T_m , because it is not possible to stop diffusion in martensite for alloys with low T_m . From Table 2, we suggest that a low M_s/T_m ratio (<0.2) is necessary in order to avoid the aging effect. It is an important guideline to design SMAs without the unwanted aging effect.

For more details on martensite aging effect, interested readers may refer to Refs. [6,89,90] for review of early work, and to Ref. [79] for a review of recent development.

3.3. Effect of deformation on martensitic transformations

When we use SMA for actuator applications, we need SMA with smaller temperature hysteresis, while when we use it for coupling applications, a larger temperature hysteresis is better. In 1986 Melton et al. [34] found that the deformation of Ti–Ni–Nb alloy in the martensitic state raised the A_f temperature greatly, and thus increases temperature hysteresis greatly, and they applied this

Table 2

Relationship between the reduced martensitic transformation temperature M_s/T_m and the rate of martensite aging (RLB) at room temperature [79]

Alloy	Ti–Ni	Cu–Al–Ni	Cu–Zn–Al	Au–Cd	In–Tl
M_s/T_m	~0.19	~0.23	~0.27	~0.34	0.50~0.79
Aging time for RLB at RT	~∞	~10 months	~5 h	~0.5 h	< 1 s

technique for pipe couplings. The mechanism for A_s increase by the deformation of martensite was explained later by the present authors [36] as follows, and it was shown that the effect is characteristic of not only Ti–Ni–Nb but also of all thermoelastic alloys. It is well-known that elastic energy is stored upon martensitic transformation. This elastic energy resists the forward transformation upon cooling, but the fact simply means that the same elastic energy assists the reverse transformation upon heating. In a more quantitative manner, Olson–Cohen [92] derived the following equation for a thermoelastic martensitic transformation by considering a thermoelastic equilibrium.

$$\Delta g_{\text{ch}} + 2\Delta g_{\text{el}} = 0$$

$$\Delta g_{\text{ch}} = g_{\text{m}} - g_{\text{p}} \quad (g_{\text{m}} \text{ and } g_{\text{p}} \text{ are free energy per unit volume in martensite and in parent, respectively})$$

Δg_{el} : elastic energy stored around martensite.

This equation means that the half of the chemical energy difference between parent and martensite is stored as elastic energy. Thus, in a thermoelastic transformation, the A_s temperature is considered to be lowered from the value characteristic of the material itself due to the presence of the elastic stored energy. Thus, if we release this elastic energy by some means, we can expect that the A_s temperature returns to the original high value. To prove that idea, the experimental result carried out for a most simple system of a Cu–Al–Ni single crystal is shown in Fig. 17(a). Fig. 17(a) indicates A_s when the specimen is subjected to a normal heating-cooling cycle. Fig. 17(b) indicates the case when it is cooled normally to multi-variants of martensite, followed by tensile testing to a single variant of martensite, and then subsequently reverse transformed by heating. Obviously A_s is raised under this condition. The reason why the A_s is raised is due to the fact that the strains in the multi-variant martensites were released from the surface of the specimen in the process of single crystallization by tension. If the specimen is once again cooled, the A_s returns to the original value as shown in Fig. 17(c),

since the specimen becomes multi-variant upon the second cooling. In the case of polycrystalline specimen, the strains can not be released from the surface. Instead the strains are released by the introduction of slip, but the process can be explained in a similar manner. Please refer to the original paper for more details [36]. In short, when a specimen is deformed in the martensitic state, A_s and A_f increase, but when it experiences a complete reverse transformation upon heating, A_s and A_f return to the original value upon the subsequent cooling. The understanding this effect will be useful in the discussion of the next section.

3.4. High temperature shape memory alloys

Although Ti–Ni alloys exhibit the best shape memory characteristics among many SMAs, as discussed in Section 2.6, they can be used up to 373 K at most. However, if SMAs, which can be used at higher temperatures, are developed, applications of SMAs will be much widened such as in engines of automobiles and in turbines of air planes etc. As such possible SMAs, we can raise Cu-based SMAs such as Cu–Zn–Al and Cu–Al–Ni, Ni–Al,

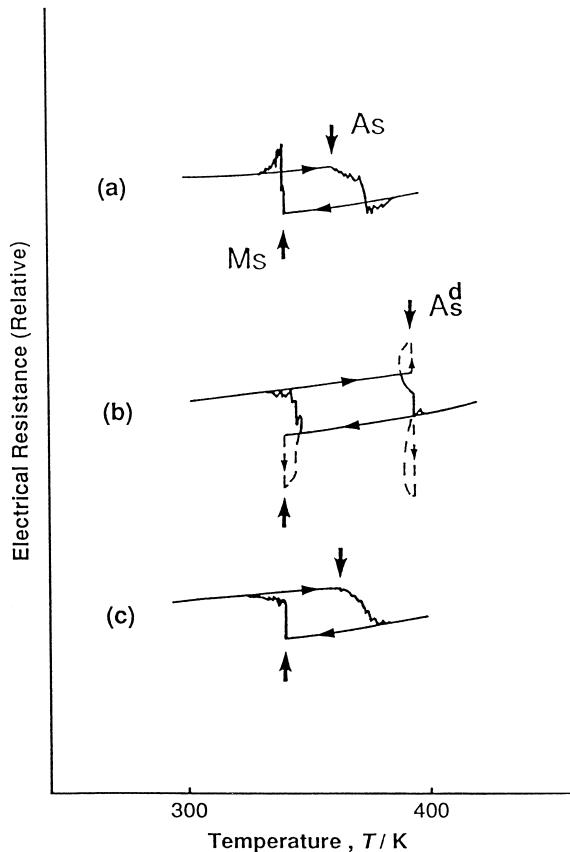


Fig. 17. Electrical resistance vs temperature curves of a Cu–13.8Al–4.0Ni (mass%) single crystal. (a) Before tensile test; (b) first cycle after tensile test in martensitic state; (c) after the cycle in (b). See text for details [36].

Ti–Ni (Zr, Hf) and Ti–Pd alloys. Among these, Cu-based alloys are not easy to keep the stable parent phase, since Cu-based alloys tend to decompose into other phases easily. Ni–Al alloys are attractive, since they are not expensive and the M_s temperature may be raised up to 1200 K, depending upon the composition [93]. However, they are brittle, and the martensite tend to transform into the Ni_5Al_3 phase instead of reverse transforming into the parent phase upon heating [94]. On the other hand, there are some reports to improve the ductility by precipitating a ductile FCC phase by the addition of Fe as a ternary element [95]. The addition of Zr or Hf to Ti–Ni alloys to raise the transformation temperature is also attractive, since Zr or Hf are relatively less-expensive. However, a brittle phase easily appear depending upon the composition, and thus it is not certain whether they can be used as practical SMA or not [96]. On the other hand, a Ti–50Pd alloy has M_s as high as 823 K, and the M_s temperature can be changed widely by replacing Pd with Ni, as shown in Fig. 18. Thus, Ti–Pd–Ni alloy system has been expected to be a hopeful candidate for high temperature SMA [98–100]. From this reason, we introduce the development of Ti–Pd–Ni SMAs in some detail in the following.

Although Ti–Pd–Ni alloys were expected as possible candidates for high temperature SMAs for many years, the actual assessments of SM characteristics at high temperature were very few until recently, since the assessment of SM characteristics at high temperature is not easy. Fig. 19 shows one example of stress-strain curves at various temperatures for a Ti–50Pd alloy, and the dotted lines in the figure represent the recovery of strain due to heating above A_f (i.e. SM strain). Surprisingly, it shows that practically no SM strains are obtained at high temperatures, although reasonably good SM strains are obtained at room temperature [101,102]. It was also confirmed that the poor SM characteristics at high temperature were due to the rapid decrease of the critical stress for slip at high temperatures

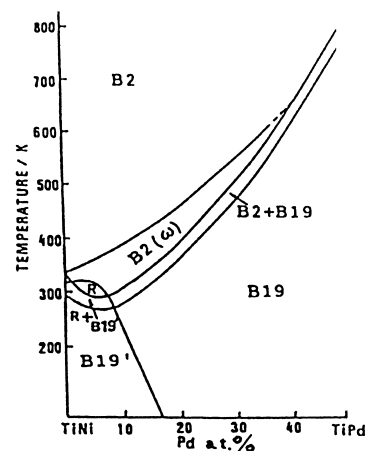


Fig. 18. Phase diagram of TiPd–TiNi alloys [97].

[101]. Thus, to improve the SM characteristics at high temperature, we can consider the following three methods.

1. thermomechanical treatment (cold working followed by suitable annealing);
2. precipitation hardening;
3. addition of quaternary element.

First we discuss the results for (i) thermomechanical treatment for Ti-(50-x)Pd-xNi alloys [103]. In short, we found that the annealing at 673 K for 1 h after cold working was very effective for the alloys for $x \leq 30$, as shown in Fig. 20. The recovery rate by SME is good only up to 2% total strain for a solution-treated specimen, but it is good up to 5.5% total strain, if the specimen is annealed at 673 K for 1 h after cold working. The superelasticity was also obtained for the specimens subjected to the above heat-treatment.

As the (ii) precipitation hardening, we tried to utilize TiB_2 by the addition of B, since the melting point of TiB_2 is very high, and the addition of B may be useful to avoid grain boundary fracture. In fact, we could obtain TiB_2 precipitates by the homogenization treatment of 1273 K for 5 h, and we could confirm that the composition is TiB_2 and the structure is PdSi_2 type by EDS (energy dispersive spectroscopy) and electron diffraction

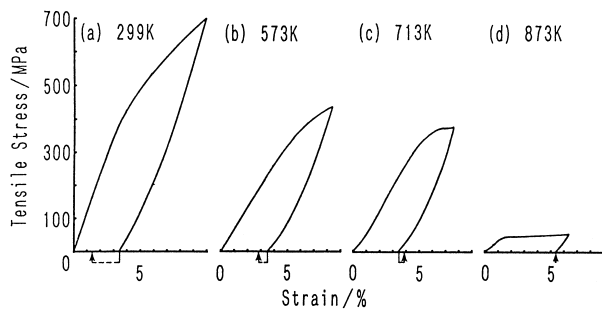


Fig. 19. Stress-strain curves of a Ti-50Pd alloy, tensile tested at various temperatures. Dotted lines with arrows indicate the strain recovered upon heating to 923 K [101].

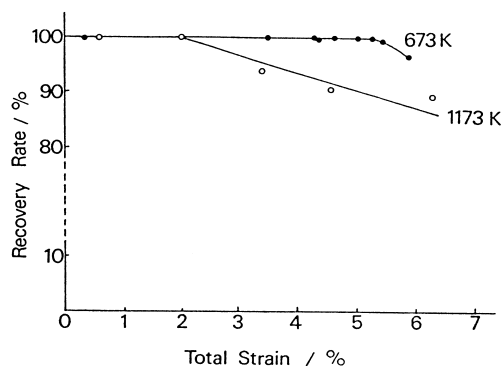


Fig. 20. Recovery rate, plotted against total strain for the solution-treated and thermomechanically treated (673 K) alloy. Tensile tests were carried out at 443 K. See text for details [103].

[104]. However, the precipitates were too big ($\sim 1 \mu\text{m}$) for precipitation hardening, although the addition of B was confirmed to be effective for improving toughness and elongation. The next problem is how to obtain small TiB_2 precipitates in a finely dispersed manner.

The result for the precipitation of TiB_2 was discussed above, and finely dispersed TiB_2 were not obtained as yet. Thus, the precipitation hardening was tried from another approach described below. We tried to introduce precipitates by shifting the Ti composition from stoichiometry such as $(50+x)\text{Ti}-30\text{Pd}-(20-x)\text{Ni}$. As a result, it was confirmed that by ageing the above alloy with $\text{Ti} > 50\text{at}\%$ at 773 K for 3.6 ks, finely dispersed precipitates appear and SM characteristics are improved [105]. However, more details await further studies.

During the course of the above study, it became necessary to study the recovery, recrystallization process of cold rolled Ti-(50-x)Pd-xNi alloys, and interesting results were obtained [106], as shown in Fig. 21. The figure shows the softening start (T_s) and softening finish (T_f) temperatures in Vickers hardness for isochronally annealed specimens for 1 h, along with A_s and A_f temperatures. We immediately notice a close correlation between the two, except for the compositions on both ends, and this correlation can be explained as follows. In this alloy system, the martensite (B19 type ordered structure) has a close-packed structure, while the parent (B2) has an open structure. Thus, diffusion is much faster in parent than in martensite. Thus, softening due to recovery-recrystallization occurs so as to follow the reverse transformation. Besides, we believe that recovery, recrystallization occurs dominantly at parent-martensite interface, where atoms are unstable and mobile. The above result clearly shows that the reverse transformation controls recovery, recrystallization processes in this alloy system, in which martensite has a closepacked structure, while parent has an open one. We now discuss the deviations of the behavior on both ends of the composition.

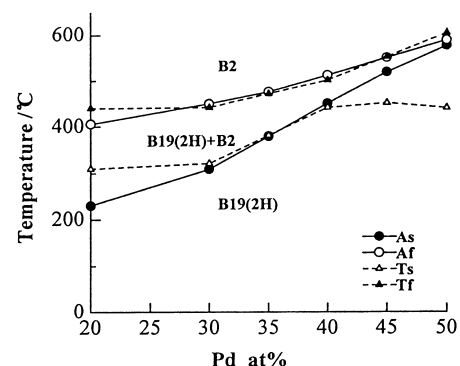


Fig. 21. Plots of reverse transformation temperatures and recovery. Recrystallization temperatures vs composition for Ti-(50-x)Pd-xNi alloys. T_s , start temperature of softening stage; T_f , finish temperature of the softening [106]. See text for details.

When Pd content is 20 at%, the temperature itself is too low even after the reverse transformation. Thus, recovery recrystallization awaits for higher temperatures. On the contrary, at 50 at% Pd, the temperature itself is high enough before reaching A_s . Thus, softening starts even below A_s , since the thermal energy is high enough. In fact, we found recrystallization in the martensitic state in a Ti–50Pd alloy [107]. The recrystallization process in the martensitic state is useful for the study of nucleation process of recrystallization, since the latter develops very slowly. See Refs. [107,108] for more details.

The above observations are useful from technological point of view also. We stated in the above that annealing at 673 K for 1 h is good for improving SM characteristics. However, this does not apply for Ti–40Pd–10Ni alloy, which is in the martensitic state, where diffusion is slow. In this case, if the alloy is flash heated to the parent phase for a very short time, and is then annealed at 673 K for 1 h, good SM characteristics are obtained. See Ref. [109] for more details.

4. Applications of shape memory alloys

Since SMAs have unique properties which ordinary metals do not have, they have high potentiality for many applications. In fact, more than 10,000 patents have been proposed in the past, and it is difficult to classify all the applications. Thus, in the following we introduce only successful applications utilizing shape memory effect and superelasticity, respectively.

4.1. Applications using shape memory effect

This type of applications may be summarized as follows.

1. couplings;
2. actuators;
3. smart materials.

Couplings are the first most successful applications of SMAs, which were developed by Raychem Corp. to hydraulic systems of F-14 jet fighters. Electric connectors for IC developed by the same company belong to the same category.

Applications as actuators were carried out in various fields such as in electric appliances, automobile devices, robotics etc. We introduce one recent example of application for a thermostatic mixing valve in Fig. 22. The apparatus consists of a SMA coil spring and a bias spring, which are opposing to each other. When the temperature of mixed water is too high, the SMA expands and the bias spring shrinks, since SMA spring is stronger than the bias spring, resulting in a smaller opening for hot-water and a larger opening for cool-water, while when the temperature of mixed water is

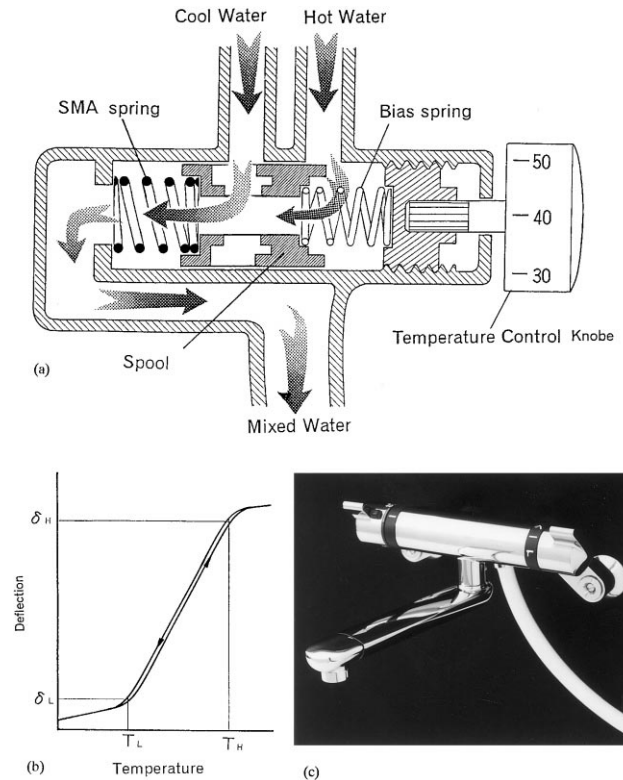


Fig. 22. The new mixing valve using SMA and biasing coil springs. (a) Represents the structure. The spool position and the mixed water temperature is controlled by varying the total length of the actuator linearly with the set temperature by the control knob. (b) Schematic representation of the temperature-deflection characteristic of the linear shape memory component used in the new mixing valve. (c) Appearance of the new mixing valve [110].

low, vice versa. In fact, it is possible to control the temperature linearly due to the Clausius-Clapeyron relationship, as shown in Fig. 22(b). Fig. 22(c) shows the appearance of this type of mixing valve. For the above purpose, wax type actuators were used in the past, but the thermal conductivity of wax is very bad, thus resulting in slow response and overshooting. On the other hand, thermal conductivity of SMA is good, resulting in excellent thermal response. Thus, the superiority of SM actuator over wax one is apparent. For more details on thermostatic mixing valve using SMA, see Ref. [110].

SMA used as an actuator described in the above has a role as a sensor as well as an actuator. Thus, SMAs are smart (or intelligent) materials. The possession of the dual function leads to the miniaturization of actuators, and thin films are expected from this point of view, as described in Section 2.7. Another type of smart materials are composites of Ti–Ni SMAs with polymer or metal matrix. The Ti–Ni wires embedded in polymers may be used for vibration control of space vehicles, since the elastic constants can be changed widely by changing the temperature in the transformation temperature range

[111]. The Ti–Ni wires embedded in Al matrix may be used to strengthen Al matrix by the same mechanism of prestressed concrete. For more details, see Ref. [112].

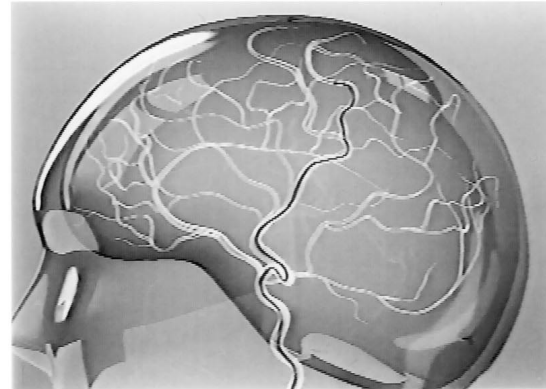
4.2. Applications using superelasticity

Superelasticity, which is a non-linear pseudoelasticity as much as 7–8%, was also successfully applied in various fields. The first application was to orthodontic arch wire, which made the orthodontic therapy much easier and effective. The second quite successful one was to brassieres for women. The third one is to the antennas for cellular phones as shown in Fig. 23. This is quite popular all over the world now, since superelastic wire is quite flexible and is not subject to damage. The fourth, which is actually the third in time sequence, is guide wires for catheters in medical use, as shown in Fig. 24. A catheter, which is a tube made of plastics, is a standard tool for diagnosing the circulatory system by injecting a contrast medium into vessels or for medical treatment by dilating a lumen of blood vessel at the site of the obstruction. To introduce the catheter in a required place of the vessel in brain, heart, liver etc., a guide wire is necessary. Previously a thin stainless steel wire was used for this purpose. However, it is being overtaken by Ti–Ni superelastic wire recently, since the latter is more flexible and is not permanently bent. Thus, this application is expanding rapidly. The above descriptions on applications of SMAs were rather sketchy. Those who are interested in more details, see Ref. [8].

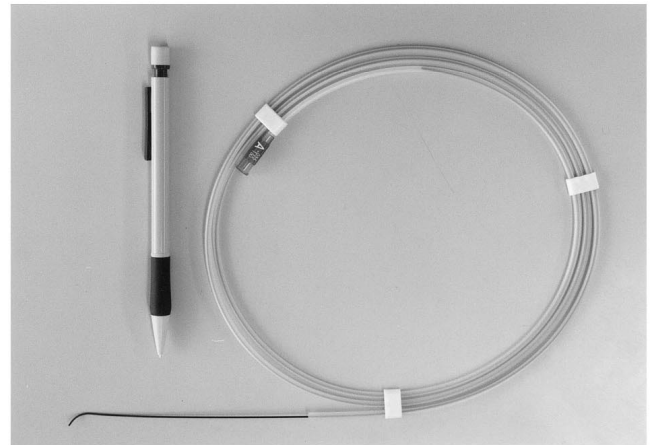
In the above, we tried to review most of the recent developments of SMAs, but we omitted some, since one of the purposes of the present overview is to introduce this field to the readers of *Intermetallics* in general. ‘Modeling of SMAs’ is such a missed topic. We also omitted the developments on Fe-based and Cu-based



Fig. 23. Superelastic antenna for a cellular phone. (Courtesy of Fujitsu Corp.)



(a)



(b)

Fig. 24. Superelastic guide wire for a catheter in medical use. (a) Applications for brain; (b) appearance of a guide wire. See text for details. (Courtesy of Terumo Corp.).

SMAs. Please see Ref. [8] for those. We also omitted technological details even for Ti–Ni and Ti–Ni based alloys. For those problems, conference proceedings are useful listed in Ref. [113–131].

As stated at the beginning, most of SMAs are intermetallics, i.e. functional intermetallics. We hope that the readers will have interest on intermetallics from this aspect as well.

Acknowledgements

The authors are grateful to Professor Tetsuro Suzuki for useful discussions on pretransformation phenomena and ductility of Ti–Ni alloys. They also appreciate the useful discussions with Mr. T. Tateishi at Terumo Corp. on medical applications. The present work was supported by Grant-in-Aid for Scientific Research on Priority, and partly supported by Project Research A from University of Tsukuba. Area on Phase Transformations (1997–9) from the Ministry of Education, Science and Culture of Japan.

References

- [1] Nishiyama Z. *Martensitic Transformations*. New York: Academic Press, 1978.
- [2] Christian JW. *The theory of transformations in metals and alloys*. Oxford: Pergamon Press, 1965.
- [3] Wayman CM. *Introduction to crystallography of martensitic transformations*. New York: MacMillan, 1964.
- [4] Warlimont H, Delaey L. *Prog Mater Sci* Vol.18, Oxford: Pergamon Press, 1974.
- [5] Otsuka K, Shimizu K. *Int Metals Rev* 1986;31(3):93.
- [6] Otsuka K, Wayman CM. In: Feltham P, editor. *Deformation behavior of materials*, vol. II. Israel: Freund Publishing House, 1977: 151.
- [7] Funakubo H. editor. *Shape memory alloys*. New York: Gordon Breach Sci Pub 1987.
- [8] Otsuka K, Wayman CM. editor. *Shape memory materials*. Cambridge: Cambridge University Press, 1998.
- [9] Massalski TB, Okamoto H, Subramanian PR, Kacprzak L. editors. *Binary alloy phase diagrams*, 2nd ed., vol. 3. Ohio: ASM International, 1990:2875.
- [10] Duez P, Taylor JL. *Trans AIME*, 1950;188:1173.
- [11] Nishida M, Wayman CM, Honma T. *Met Trans* 1986;17A:1505.
- [12] Honma T, Matsumoto T, Shugo Y, Nishida M. *Res Rep Nucl Sci Lab Tohoku Univ* 1979;12(2):183.
- [13] Miyazaki S, Ohmi Y, Otsuka K, Suzuki Y. *J de Phys Colloque C4, Suppl. No. 12, 1982*;43:C4–255.
- [14] Saburi T, Tatsumi T, Nenno S. *ibid.* C4–261.
- [15] Tadaki T, Nakata Y, Shimizu K, Otsuka K. *Trans Jpn Inst Metals* 1986;27:731.
- [16] Saburi T, Nenno S, Fukuda T. *J Less-Com Metals* 1986;125:157.
- [17] Hara T, Ohba T, Otsuka K. *Mater Trans JIM* 1997;38:277.
- [18] Kudoh Y, Tokonami M, Miyazaki S, Otsuka K. *Acta Metall* 1985;33:2049.
- [19] Matsumoto M, Honma T. *New aspects of martensitic transformations*. First Jpn. Inst. Metals Int. Symp. on Martensite, Kobe, Japan. *Jpn Inst Metals Sendai* 1976: 199.
- [20] Hwang CM, Wayman CM. *Scripta Metall* 1983;17:381.
- [21] Miyazaki S, Otsuka K. *Met Trans* 1986;17A:53.
- [22] Miyazaki S, Otsuka K. *Phil Mag A* 48;1984:393.
- [23] Hara T, Ohba T, Okunishi E, Otsuka K, *Mater Trans JIM* 1997;38:11.
- [24] Ohba T, Emura Y, Otsuka, K. *Mater Trans JIM* 1992;33:29.
- [25] Hwang CM, Meichle M, Salamon MB, Wayman CM. *Phil Mag* 1983;47:9.
- [26] Nakanishi N. *Prog Mater Sci*, Pergamon Press 1980;24:143.
- [27] Mercier O, Melton KN, Gremaud G, Hagi J. *J Appl Phys* 1980;51:1833.
- [28] Khachin VN, Muslov SA, Pushin VG, Chumlyakov Yu.I. *Sov Phys Dokl* 1987;32:606.
- [29] Brill TM, Mittelbach SM, Assmus W, Müllner M, Lüthi B. *J Phys Condens Matter* 1991;3:9621.
- [30] Ren X, Taniwaki K, Otsuka K, Suzuki T, Tanaka K, Chumlyakov Yu.I, Ueki T. *Phil Mag A* 1998; in press.
- [31] Ren X, Otsuka K. *Scripta Mater* 1998;38:1669.
- [32] Planes A, Manosa L, Vives E. *Phys Rev* 1996;53B:3039.
- [33] Nam TH, Saburi T, Shimizu K. *Mater Trans JIM* 1990;31:959.
- [34] Melton KN, Simpson J, Duerig TW. *Proc Int Conf on Martensitic Transformations (ICOMAT-86)*. *Jpn Inst Metals* 1986:1053.
- [35] Zhao LC, Duerig TW, Wayman CM. *Proc MRS Int Mtg on Adv Mats*, Tokyo 1989:171.
- [36] Piao M, Otsuka K, Miyazaki S, Horikawa H. *Mater Trans JIM* 1993;34:919.
- [37] Matsumoto O, Miyazaki S, Otsuka K, Tamura H. *Acta Metall* 1987;35:2137.
- [38] Miyazaki S, Otsuka K, Wayman CM. *Acta Metall* 1989;37:1873.
- [39] Fukuda T, Saburi T, Doi K, Nenno S. *Mater Trans JIM* 1992;33:271.
- [40] Onda T, Bando Y, Ohba T, Otsuka K. *Mater Trans JIM* 1992;33:354.
- [41] Knowles KM, Smith DA. *Acta Metall* 1981;29:101.
- [42] Nishida M, Ohgi H, Itai I, Chiba A, Yamauchi K. *Acta Metall Mater* 1995;43:1219.
- [43] Hara T, Ohba T, Otsuka K, Bando Y, Nenno S. *Proc ICOMAT-92, Monterey* 1992:257.
- [44] Miyazaki S, Otsuka K, Suzuki Y. *Scripta Metall* 1981;15:287.
- [45] Miyazaki S, Kohiyama Y, Otsuka K. *Proc Int Symp on Intermetallic Compounds JIMIS-6, Sendai, 1991*:691.
- [46] Miyazaki S, Matsumoto O, Otsuka K. *ibid.*:269.
- [47] Goo E, Duerig T, Melton K, Sinclair R. *Acta Metall* 1985;33:1725.
- [48] Laves F. *Naturwissenschaften* 1952;39:546.
- [49] Cahn RW, Coll JA. *Acta Metall* 1961;9:138.
- [50] Furuya Y, Matsumoto M, Kimura HS, Aoki K, Masumoto T. *Mater Trans JIM* 1990;31:504.
- [51] Busch AD, Johnson AD, Lee CH, Stevenson DA. *J Appl Phys* 1990;68:6224.
- [52] Miyazaki S, Ishida A, Takei A. *Proc ICOMAT-92* 1993:893.
- [53] Miyazaki S, Hashinaga T, Yumikura H, Horikawa H, Ueki T, Ishida S. *Smart Materials*. *SPIE Proc Series* 2441 1995:156.
- [54] Miyazaki S, Nomura K, Ishida A. *J de Physique Colloque IV. Proc. ICOMAT-95. C8, 1995*;5:677.
- [55] Kawamura Y, Gyobu, S, Horikawa H, Saburi T. *J de Physique Colloque IV. Proc. ICOMAT-95. C8, 1995*;5:683.
- [56] Nakata Y, Tadaki T, Sakamoto H, Tanaka A, Shimizu, K. *J de Physique Colloque IV. Proc ICOMAT-95. C8, 1995*;5:671.
- [57] Kohl M, Shrobanek KD, Quandt E, Schlossmacher P, Schussler A, Allen DM. *J de Physique Colloque IV. (Proc. ICOMAT-95). C8, 1995*;5:1187.
- [58] Hou Li, Grummon DS. *Scripta Metall et Mater* 1995;33:989.
- [59] Ishida A, Sato M, Takei A, Miyazaki S. *Mater Trans JIM* 1995;36:1349.
- [60] Gyobu A, Kawamura Y, Horikawa H, Saburi T. *Mater Trans JIM* 1996;37:697.
- [61] Kajiwara S, Kikuchi T, Ogawa K, Matsunaga T. *Phil Mag Lett* 1996;74:137.
- [62] Kajiwara S, Ogawa K, Kikuchi T, Matsunaga T, Miyazaki S. *Phil Mag Lett* 1996;74:395.
- [63] Ishida A, Takei A, Sato M, Miyazaki, S. *Thin Solid Films* 1996;281–282:337.
- [64] Ishida A, Sato M, Takei A, Nomura K, Miyazaki S. *Metall Trans Mater A* 1996;27A:3753.
- [65] Grummon DS, Pence TL. *MRS Symp Proc* 1997;459:331.
- [66] Tan S. Ph.D. thesis, University of Tsukuba 1998:98.
- [67] Nakata Y, Tadaki T, Hirotsu Y, Sakamoto H, Shimizu K. *Collected Abstracts of the Annual Fall Meeting of Jpn Inst Metals*, Sapporo 1996:165.
- [68] Kahn H, Benard WL, Huff MA, Heuer AH. *MRS Symp Proc* 1997;444:227.
- [69] Nagpal P, Baker I. *Met Trans* 1990;21A:2281.
- [70] Zener C. *Phys Rev* 1947;71:846.
- [71] Krumhansl JA. *Sol Stat Comm* 1992;84:251.
- [72] Ren X, Kawano T, Otsuka K, Kogachi M. *Collected Abstracts of Annual Spring Meeting of Jpn Inst Metals, Tokyo* 1997:81.
- [73] Neuman JP. *Acta Metall* 1980;28:1165.
- [74] Kogachi M, Tanahashi T, Shirai Y, Yamaguchi M. *Scripta Mater* 1996;34:243.
- [75] Kogachi M, Tanahashi T. *Scripta Mater* 1996;35:849.

- [76] Kogachi M, Haraguchi T, Kim SM. *Intermetallics* 1998;6:499.
- [77] Ren X, Otsuka K, Kogachi M. Collected Abstracts of Annual Fall Meeting of Jpn. Inst. Metals, Sendai 1997:401.
- [78] Murakami Y, Nakajima Y, Otsuka K. *J de Phys III* 1995;5:C8–1071.
- [79] Ren X, Otsuka K. *Phase Transitions* 1998 (in press).
- [80] Barcelo G, Rapacioli R, Ahlers M. *Scripta Metall* 1978;12:1069.
- [81] Murakami Y, Nakajima Y, Otsuka K, Ohba T. *J de Phys III* 1995;5(C8):1071.
- [82] Ohba T, Otsuka K, Sasaki S. *Mater Sci Forum* 1990;56–58:317.
- [83] Ohba T, Finlayson T, Otsuka K. *J de Phys III* 1995;5(C8):1083.
- [84] Ahlers M, Barcelo G, Rapacioli R. *Scripta Metall* 1978;12:1075.
- [85] Marukawa K, Tsuchiya K. *Scripta Metall* 1995;32:77.
- [86] Ren X, Otsuka K. *Nature* 1997;389:579.
- [87] Bradley AJ, Taylor A. *Proc Roy Soc London* 1937;A159:56.
- [88] Christian JW. *The theory of transformations in metals and alloys*. Oxford: Pergamon Press, 1965:789.
- [89] Ahlers M. *Proc ICOMAT'86*. Jpn Inst Met 1986:786.
- [90] Tadaki T, Otsuka K., Shimizu K. *Ann Rev Mater Sci* 1988;18:25.
- [91] Kozuma M, Murakami Y, Otsuka, K. *Proc Int Conf on Displacive Phase Transformations and Their Applications in Materials Engineering*, TMS 1998:233.
- [92] Olson GB, Cohen M. *Scripta Metall* 1975;9:1247.
- [93] Smialek JL, Hchemann RF. *Met Trans* 1973;4:1571.
- [94] Yang JH, Wayman CM. *Intermetallics* 1994;2:111.
- [95] Kainuma R, Ishida K, Nishizawa T. *Met Trans* 1992;23A:147.
- [96] Mulder JH, Maas JH, Beyer J. *Proc. ICOMAT-92*. Monterey, 1992 869.
- [97] Matveeva NA, Kovneristy Yu.K, Savinov AS, Sivokha VP, Khachin VN. *J Phys* 1982;43:Suppl. 12 C4–249.
- [98] Donkersloot HC, Van Vucht JHN. *J. Less-Com Metals* 1970;20:83.
- [99] Khachin VN, Matveeva NA, Sivokha VP, Chernov DV. *Acad Nauk SSSR* 1981;257:167.
- [100] Enami K, Hoshiya T. *Proc Mat Tech '90*, 1990:1.
- [101] Otsuka K, Oda K, Ueno Y, Piao M, Ueki T, Horikawa H. *Scripta Metall & Mater* 1993;29:1355.
- [102] Hoshiya T, Enami K, Yamauchi K. *Advanced Materials '93 V/B: Shape Memory Materials and Hydrides* (editors. Otsuka, K. et al.) *Trans MRS-Japan* 18B. Amsterdam: Elsevier Science, 1013.
- [103] Golberg D, Xu Ya, Murakami Y, Morito S, Otsuka K, Ueki T, Horikawa H. *Scripta Metall et Mater* 1994;30:1349.
- [104] Suzuki Y, Xu Ya, Morito S, Otsuka K, Mitose K. *Mater Lett* 1998;36:85.
- [105] Shimizu S, Xu Ya, Okunishi E, Tanaka S, Otsuka K, Mitose K. *Mater Lett* 1998;34:23.
- [106] Xu Ya, Shimizu S, Suzuki S, Otsuka K, Ueki T, Mitose K. *Acta Mater* 1997;45:1503.
- [107] Xu Ya, Otsuka K, Furubayashi E, Ueki T, Mitose K. *Mater Lett* 1997;30:189.
- [108] Xu Ya, Otsuka K, Furubayashi E, Mitose K. *Mater Lett* 1998;34:14.
- [109] Golberg D, Xu Ya, Murakami Y, Otsuka K, Ueki T, Horikawa H. *Mater Lett* 1994;22:241.
- [110] Ohkata H, Tamura H. *MRS Symp Proc* 1997;459:345.
- [111] Schetky L. McD. *MRS Symp Proc* 1992;246:299.
- [112] Furuya Y, Sasaki A, Taya M. *Trans. JIM*, 1993; 34: 224.
- [113] Suzuki H. editor, *Proc 1st JIM Int Symp on New Aspects of Martensitic Transformations*. ICOMAT-76, Jpn Inst Met Sendai 1976.
- [114] Owen WS. et al. editor, *Proc Int Conf on Martensitic Transformations*. ICOMAT-79, Cambridge, Massachusetts, 1979.
- [115] Delaey L, Chandrasekaran S. *J de Phys. Proc. ICOMAT-82*, 43, Suppl. 12, 1982.
- [116] Tamura I, editor, *Proc Int Conf on Martensitic Transformations*. ICOMAT-86, Jpn. Inst. Met., Sendai, 1987.
- [117] Muddle BC, editor, *Martensitic Transformations*. *Proc ICOMAT-89*, *Mater Sci Forum* 1990:56–8.
- [118] Wayman CM, Perkins J. editor, *Proc Int Conf on Martensitic Transformations*. ICOMAT-92, Monterey Institute of Advanced Studies, Carmel, CA, 1993.
- [119] Gotthardt R, Van Humbeeck J. *Proc Int Conf on Martensitic Transformations*. ICOMAT-95, Suppl J de Phys, 1995:III, No. 12.
- [120] Otsuka K, Shimizu K. editors, *Proc MRS Int Meeting on Adv Mater* 9. Tokyo, 1988, MRS, Pittsburgh, 1989.
- [121] Liu CT, Kunsmann H, Otsuka K, Wuttig M. editors, *Shape memory materials—Fundamental aspects and applications*. *MRS Symp Proc* 1992:246.
- [122] Otsuka K, Fukai Y. editors, *Shape memory materials and hydrides, advanced materials '93/B*, 18B (Elsevier, Amsterdam, 1994).
- [123] George EP, Takahashi S, McKinstry ST, Uchino K, Wun-Fogle M. editors, *Materials for Smart Systems*. *MRS Symp Proc* 1995:360.
- [124] George EP, Gotthardt R, Otsuka K, Troiler-McKinstry S, Wun-Fogle M. editors, *Materials for Smart Systems II*. *MRS Symp Proc* 1997:459.
- [125] Perkins J. editor, *Shape memory effect in alloys*. New York: Plenum Press, 1975.
- [126] Duerig TW, Melton KN, Stockel D, Wayman CM, editors, *Engineering aspects of shape memory alloys*. London, Butterworth-Heinemann, 1990.
- [127] Hornbogen E, Jost N, editors, *The Martensitic Transformation in Science and Technology*. Oberursel, Informationsgesellschaft: 1989.
- [128] Chu Youyi, Hsu TY, Ko T, editors, *Proc Int Symp on Shape Memory Alloys* (Guilin, 1986), (China Academic Pub., 1986).
- [129] Chu Youyi, Tu Hailing ed., *Proc. Int. Symp. on Shape Memory Materials*. Beijing, 1994, International Academic Pub., Beijing, 1994.
- [130] Pelton AR, Hodgson D, Duerig T, editors, *Proc 1st Int Conf on Shape Memory and Superelastic Technologies*. NDC, Inc., Fremont, California, 1995.
- [131] Inoue K, Mukherjee K, Otsuka K, Chen H. *Proc Int Conf on Displacive Phase Transformations and their Applications in Materials Engineering*, TMS, 1998.